GeoScienceWorld
Lithosphere
Volume 2022, Article ID 8127747, 11 pages
https://doi.org/10.2113/2022/8127747

Lithosphere

Research Article

First *In Situ* Terrestrial Osbornite (TiN) in the Pyrometamorphic Hatrurim Complex, Israel

Evgeny Galuskin,[1] **Irina O. Galuskina**,[1] **Vadim Kamenetsky**,[2] **Yevgeny Vapnik**,[3] **Joachim Kusz**,[4] **and Grzegorz Zieliński**[5]

[1]*Faculty of Natural Sciences, Institute of Earth Sciences, University of Silesia, Poland*
[2]*Institute of Experimental Mineralogy RAS, 142432 Chernogolovka, Russia*
[3]*Department of Geological and Environmental Sciences, Ben-Gurion University of the Negev, PO Box 653 Beer-Sheva 84105, Israel*
[4]*Faculty of Science and Technology, University of Silesia, ul. 75. Pułku Piechoty 1, 41-500 Chorzów, Poland*
[5]*Polish Geological Institute-National Research Institute, Rakowiecka 4, 00-975 Warsaw, Poland*

Correspondence should be addressed to Evgeny Galuskin; evgeny.galuskin@us.edu.pl

Received 22 October 2022; Revised 2 December 2022; Accepted 12 December 2022; Published 31 December 2022

Academic Editor: Francis McCubbin

Osbornite (TiN) is extremely rare in nature (commonly found in enstatite meteorites) and has not yet been identified correctly to form naturally in terrestrial settings. Due to its thermodynamic stability and thermal shock resistance, TiN has wide industrial applications, mainly as coatings. However, as the melting temperature of TiN is very high (~3000°C), coatings are produced at much lower temperatures via physical or chemical vapor deposition. Also, anthropogenic analogues of osbornite are often observed in pyrometallurgical slags. Therefore, it is critical to distinguish between anthropogenic and naturally occurring osbornite. A detailed petrographic study was undertaken on *in situ* osbornite found within unusual gehlenite-bearing breccias from wadi Zohar, Negev Desert of the pyrometamorphic Hatrurim Complex. The Hatrurim Complex, which extends through Israel, Palestine, and Jordan within the Dead Sea Rift zone, mainly comprises larnite, gehlenite, and spurrite rocks. Osbornite, in close association with iron phosphides, barringerite, and schreibersite, occurs at contacts between gehlenite, paralava, and calcinated clasts of host sedimentary rocks. Based on investigation of pseudowollastonite and Fe-P series phases, osbornite is formed at low pressure, extremely high temperatures (~1200-1500°C), and reduced conditions, following pyrolysis of organic matter contained in the sedimentary protolith. This is the first identification of *in situ* osbornite in terrestrial rocks and indicates that high-temperature and highly reduced conditions, which are common for meteorites, may occur at/near the Earth's surface as a result of sustained pyrometamorphism in particular settings. Our findings also provide relevant data and criteria for comparing osbornite occurrences elsewhere and ultimately evaluating their origins.

1. Introduction

Nitrogen is a typical component of organic minerals and inorganic N-bearing minerals, in which it is usually present as ammonium or nitrate complexes. In contrast, nitrides are exceptionally rare in nature and generally have extraterrestrial origins. The following nitrides have been documented in meteorites: nierite, Si_3N_4 [1]; sinoite, Si_2N_2O [2]; roaldite, γ-Fe_4N [3]; carlsbergite, CrN [4]; uakitite, VN [5]; and osbornite, TiN [6]. The few exceptional terrestrial findings of nitrides include siderazot, $Fe_3N_{1.33}$ in volcanic materials of Mt. Etna, Sicily [7] and oreillyite, Cr_2N [8] and qingsongite, BN [9] reported in heavy mineral separates from Mt. Carmel, Israel and Loubousa chromitites, Tibet, China, respectively. There have also been the discovery of low-temperature nitride-bearing mercury minerals such as gianellaite, $(Hg_2N)_2SO_4$ [10]; kleinite, $Hg_2N((SO_4)_{0.25}Cl_{0.5})\cdot 0.5H_2O$ [11]; mosesite, $Hg_2N(Cl,SO_4,MoO_4,CO_3)\cdot H_2O$ [12]; and comancheite, $Hg_{55}N_{24}(OH,NH_2)_4(Cl,Br)_{34}$ [13] from Terlingua, Brewster County, Texas, USA.

Natural titanium nitride, osbornite, (TiN) was first described in 1852 from a meteorite (aubrite) which fell near

Bustree, India [6]. Since then, osbornite has been routinely identified in enstatite meteorites [14–16] and was also found in the 81P/Wild 2 comet dust [17].

TiN is implemented in a range of industries owing to its thermodynamic stability, thermal resistance, and robustness under mechanical stress [18–20]. Extensive applications of TiN coatings include cutting tools, extrusion castings, automotive and aerospace parts, computer disk drives, precision and surgical/medical instruments, and artificial human organs. These coatings are produced using physical or chemical vapor deposition processes [20]. Anthropogenic analogues of osbornite are common in slags from metal and special ceramic production processes [21–24]. Mass production and high stability of titanium nitride may cause environmental pollution by artificial TiN grains, similarly to technogenic diamond, silicon carbide (moissanite), corundum, etc. [25–27]. In contrast to these other anthropogenic analogues, the bulk of anthropogenic TiN particles from industrial coatings is nanosized and is thus unlikely to be detected in natural objects. However, larger grains that form intergrowths or inclusions in slag products [21–24], such as iron or corundum, can often survive in natural settings. In fact, osbornite on Earth has exclusively been found in mineral separates from bulk rock samples, in which its micrometre- and nanometre-sized inclusions are mainly hosted in corundum [28–44] and are thus unsupportive of natural origins [27, 45].

Osbornite has recently been discovered *in situ* within gehlenite-bearing breccias of the Hatrurim Complex, Israel, in association with "meteorite"-type phosphides, such as schreibersite, barringerite, allabogdanite, and andreyivanovite [46]. Here, we investigate the terrestrial origins of *in situ* osbornite by studying its mineral associations, composition, structure, and Raman shift. In addition, we discuss the physicochemical conditions and formation mechanisms for osbornite and associated phosphides, with implications for the petrogenesis of the Hatrurim Complex.

2. Background Information

2.1. Hatrurim Complex. The pyrometamorphic Hatrurim Complex (Mottled Zone) comprises larnite-, spurrite- and gehlenite-bearing rocks which form large outcrops (up to 100 s of km^2) along the Dead Sea Rift zone in the territories of Israel, Jordan, and Palestine [47–51]. These lithologies formed under oxidizing, sanidinite facies metamorphic conditions (700-1400°C and low pressure) and therefore contain minerals with predominantly trivalent iron [52]. Pyrometamorphism of the Hatrurim Complex was initially proposed to occur from the burning of bitumen-rich protoliths [48]; recently, proposed hypothesis of the "mud volcanoes" has shown that fire activation and protolith transformation was the result of methane delivery via supply channels from gaseous traps within the tectonically active zone of the Dead Sea Rift [50, 53]. Moreover, this transformation process involved the combustion of by-products (gases, fluids, and melts) at high temperatures which reacted with minerals of the early "clinker association" and significantly increased the mineral diversity within the complex, including the reduced phosphide associations [46, 54, 55].

Phosphide-bearing rocks were found at three localities within the Hatrurim Complex: Daba Siwaqa, Jordan (N31.367°, E36.187°), the Hatrurim Basin, Negev Desert, Israel: wadi Halamish (N31.161°, E35.301°) and wadi Zohar (N31.183°, E36.291°) [46, 54, 56]. In Jordan, phosphides were observed in diopside paralava within bedrock [54, 57, 58], whereas Israeli findings of phosphide-bearing rocks were found *ex situ* at the wadi Halamish (diopside paralava) and wadi Zohar (gehlenite breccia) [54, 56, 57, 59]. In 2019, we were able to find a bedrock source of phosphide-bearing gehlenite breccia, which contains numerous osbornite grains [46].

2.2. Samples and Methods of Investigation. More than 300 samples of phosphide-bearing breccia were collected during field trips in 2019 and 2021, and in the 13 samples, osbornite was revealed. Unambiguously natural terrestrial origin of osbornite is carefully monitored by observing and sampling the mineral grains at different levels from the outcrop to hand specimen and thin sections (Figure 1).

The morphology and chemical composition of osbornite and associated minerals were investigated using Philips XL30, Phenom XL, and Quanta 250 EDS-equipped scanning electron microscopes (Institute of Earth Sciences, University of Silesia, Poland). The chemical composition of osbornite was measured with a CAMECA SX100 electron microprobe analyzer (EMPA, Micro-Area Analysis Laboratory, Polish Geological Institute—National Research Institute, Warsaw, Poland): WDS, accelerating voltage = 15 kV, beam current = 40 nA, beam diameter~2 μm. The following standards and lines were used: apatite = Ca$K\alpha$; rutile = Ti$K\alpha$; hematite = Fe$K\alpha$; V metal = V$K\alpha$; Cr_2O_3 = Cr$K\alpha$; BN = N$K\alpha$; sanidine = Al$K\alpha$; and diopside = Si$K\alpha$.

Raman spectra of osbornite and associated minerals were recorded on a WITec alpha 300R Confocal Raman Microscope (Institute of Earth Sciences, University of Silesia, Poland) equipped with an air-cooled solid laser (532 nm) and a CCD camera operating at –61°C. An air Zeiss LD EC Epiplan-Neofluar DIC-100/0.75NA objective was used. Raman-scattered light was focused through a broad band single mode fibre with an effective pinhole size about 30 μm and a monochromator with a 600 mm^{-1} grating. The power of the laser at the sample position was ~10-15 mW. Integration times of 3 s with accumulation of 30 scans were chosen, and the resolution is 3 cm^{-1}. The monochromator was calibrated using the Raman scattering line of a silicon plate (520.7 cm^{-1}).

Single-crystal X-ray study of osbornite crystal was carried out using a SuperNova diffractometer with a mirror monochromator (MoKα, λ = 0.71073 Å) and an Atlas CCD detector (Agilent Technologies) at the Institute of Physics, University of Silesia, Poland. The osbornite structure was refined using the SHELX-97 program [60].

3. Osbornite and Rock Description

Osbornite grains up to 40 μm in size were found in phosphide-bearing explosive breccia forming vertical zone

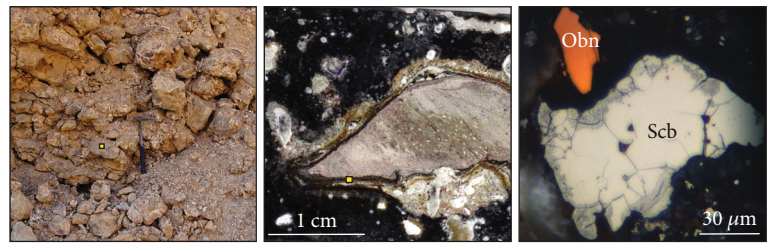

FIGURE 1: (a) Outcrop of phosphide-bearing breccia. Sampling location is given by the yellow square, fragment of which is presented in (b). (b) Polished fragment of rock with pink xenolith in gehlenite paralava. Yellow square indicates an area magnified in (c). (c) Osbornite grain within a phosphide-rich domain. Reflected light. Obn = osbornite; Scb = schreibersite.

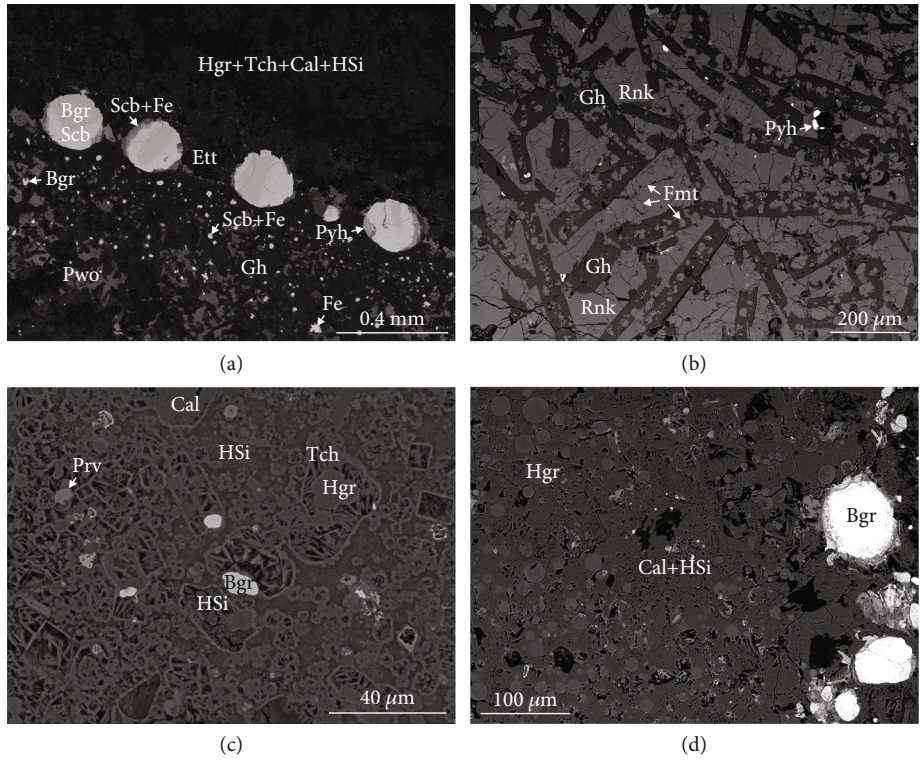

FIGURE 2: Back-scattered electron (BSE) images of paralava, host rock, and breccias. (a) Rounded polymineral Fe-(±C)-phosphide aggregates occurring at the boundary between paralava and the host rock. (b) Rankinite-gehlenite paralava with flamite relics. (c) Hydrogrossular-hydrosilicate rock, which formed as result of hydration of thermally altered fragments of host rock. (d) Rare, rounded hydrogrossular-like phases within calcite-hydrosilicate cement at the contact with paralava. Bgr = barringerite; Cal = calcite; Ett = ettringite; Fe = native Fe; Fmt = flamite; Gh = gehlenite; Hgr = hydrogrossulare; HSi = undiagnosed hydrosilicate; Prv = perovskite; Pwo = pseudowollastonite; Pyh = pyrrhotite; Rnk = rankinite; Scb = schreibersite; Tch = acharanite.

4-5 m in width in layered pinkish low-temperature Hatrurim Complex rocks at the Arad-Dead Sea road, wadi Zohar, Negev Desert, Israel [46]. The breccia comprises hydrogrossular-bearing porous clasts of the altered host rock cemented by a gehlenite-bearing paralava matrix, which also have large (up to 1.5 cm) polymineral Fe-(±C)-phosphide aggregates along clast boundaries [46]. These rounded aggregates consist of barringerite, Fe_2P_{hex}; schreibersite, Fe_3P; native iron, α-Fe; and eutectic schreibersite-iron (± cohenite), in which thin murashkoite, FeP, zones are sporadically observed (Figure 2(a); Table S1). Moreover, V-Cr-bearing allabogdanite, Fe_2P_{rhomb}, and V-bearing andreyivanovite, FeCrP were found in narrow tongues of paralava enriched in pseudowollastonite, together with barringerite [46].

The host rocks are hydrated and porous and composed primarily of hydrogrossular, hydrosilicates (tacharanite, $Ca_{12}Al_2Si_{18}O_{33}(OH)_{36}$; tobermorite, $Ca_4Si_6O_{17}(H_2O)_2{\cdot}(Ca{\cdot}3H_2O)$; afwillite, $Ca_3[SiO_3(OH)]_2{\cdot}2H_2O)$), and calcite. They were formed as a result of low-temperature alteration of

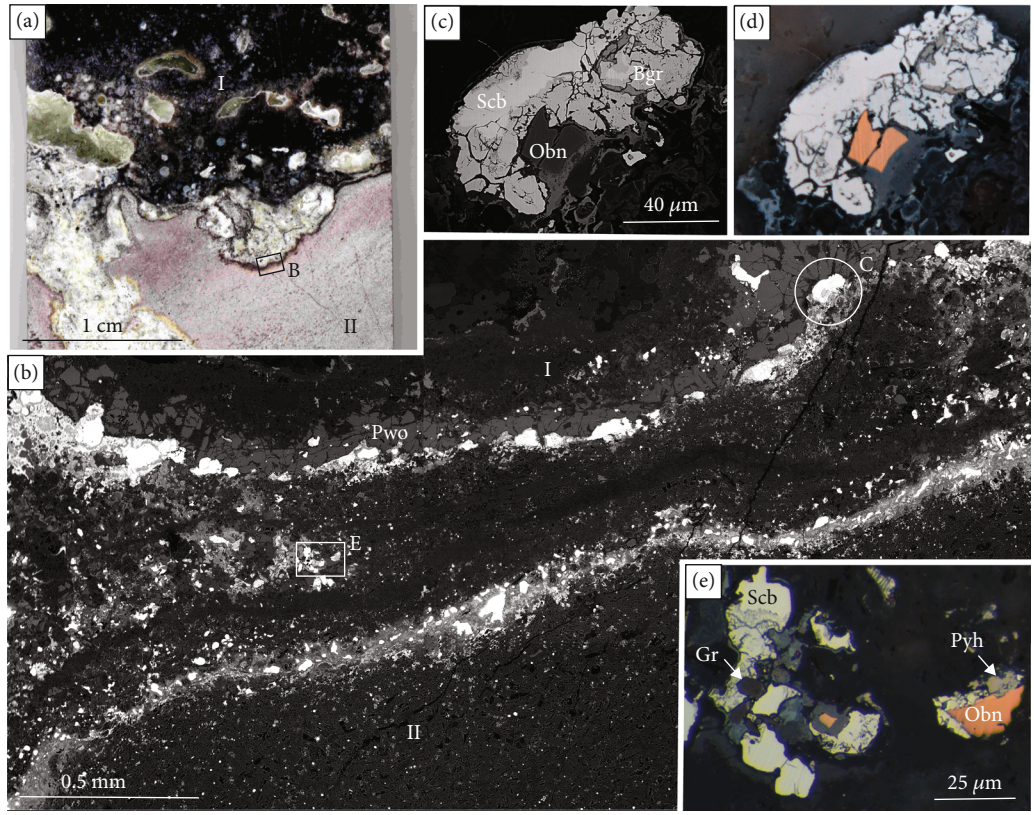

FIGURE 3: Scanned section (a), optical light microscopy (d), and BSE (b, c, e) images of contact between paralava and host rock. (a) Low-resolution image showing contact between paralava (I) and host rock (II) with gaseous channels containing ettringite, gypsum, or calcite. Lighter fragments of paralava are pseudowollastonite-rich and contain hydrogrossular which has replaced gehlenite. The area of (B) is shown in the frame. (b) Overview of contact (paralava (I) and hydrogrossular-bearing rock (II)) enriched in phosphides, native iron, and products of their alteration (lighter phases). Areas magnified in (C) and (E) are indicated by the circle and frame, respectively. (c, d) Osbornite crystal intergrown with barringerite and schreibersite. (e) Rare graphite crystals in association with osbornite, schreibersite, and pyrrhotite. Bgr = barringerite; Gr = graphite; Obn = osbornite; Pwo = pseudowollastonite; Pyh = pyrrhotite; Scb = schreibersite.

pyrometamorphic clinker-like rocks of the Hatrurim Complex, which were originally sedimentary rocks of the Gareb Formation (Maastrichtian) [48, 49, 61, 62].

Gehlenite-bearing paralava is extremely heterogeneous with respect to mineral composition and texture, and amygdaloidal types of paralava are often observed. Gehlenite-flamite paralava represent the least altered type [46]. Progressive alteration leads to the replacement of flamite (α'-Ca_2SiO_4 stabilized by the P, Na, and K impurities) by rankinite ($Ca_3Si_2O_7$) within central fragments of paralava (Figure 2(b); Figure S1), which is then completely replaced by pseudowollastonite and cuspidine (which also crystallizes along walls of the gaseous channels) at the contact with the host rock. At clast boundaries within the breccia, gehlenite in paralava is completely replaced by hydrogrossular. Accessory minerals of gehlenite-bearing paralava include fluorapatite, Si-bearing perovskite, Cr-Fe-spinel, pyrrhotite, native iron and occasional sphalerite, and wüstite. Phosphides rarely occur within the paralava and are generally restricted to the porous fragments of the rock. Unlike paralava, all host rock clasts have been recrystallized into fine-grained, porous rocks consisting of hydrogrossular, tacharanite, and tobermorite-like hydrosilicates (Figure 2(c)). Case-like pseudomorphs within these clasts are rectangular or square, which may indicate a possible precursor gehlenite, while the presence of small grains (<10 μm) of iron phosphides (usually, barringerite), native iron, baghdadite, zirconolite, cuspidine, and pseudowollastonite may represent potential relics of high-temperature metamorphism (Figure 2(c); [46]). The sedimentary protoliths of the host rocks were most likely altered to clinker-like rock prior to entrainment within gehlenite paralava. At the contact zone between paralava and breccia, small (20-30 μm) rounded grains with compositions close to hydrogrossular are dispersed throughout the calcite-hydrosilicate matrix (Figure 2(d)). The morphology of these grains supports formation via melting of clinker-like fragments at the contact with paralava, which were subsequently replaced by secondary minerals.

Geochemical data indicate that gehlenite paralava and hydrogrossular-bearing host rock fragments were derived from the same protolith [46].

Relatively large (up to 30 μm), rare osbornite grains are found exclusively at the contact between paralava and small host rock clasts, where they form intergrowths with

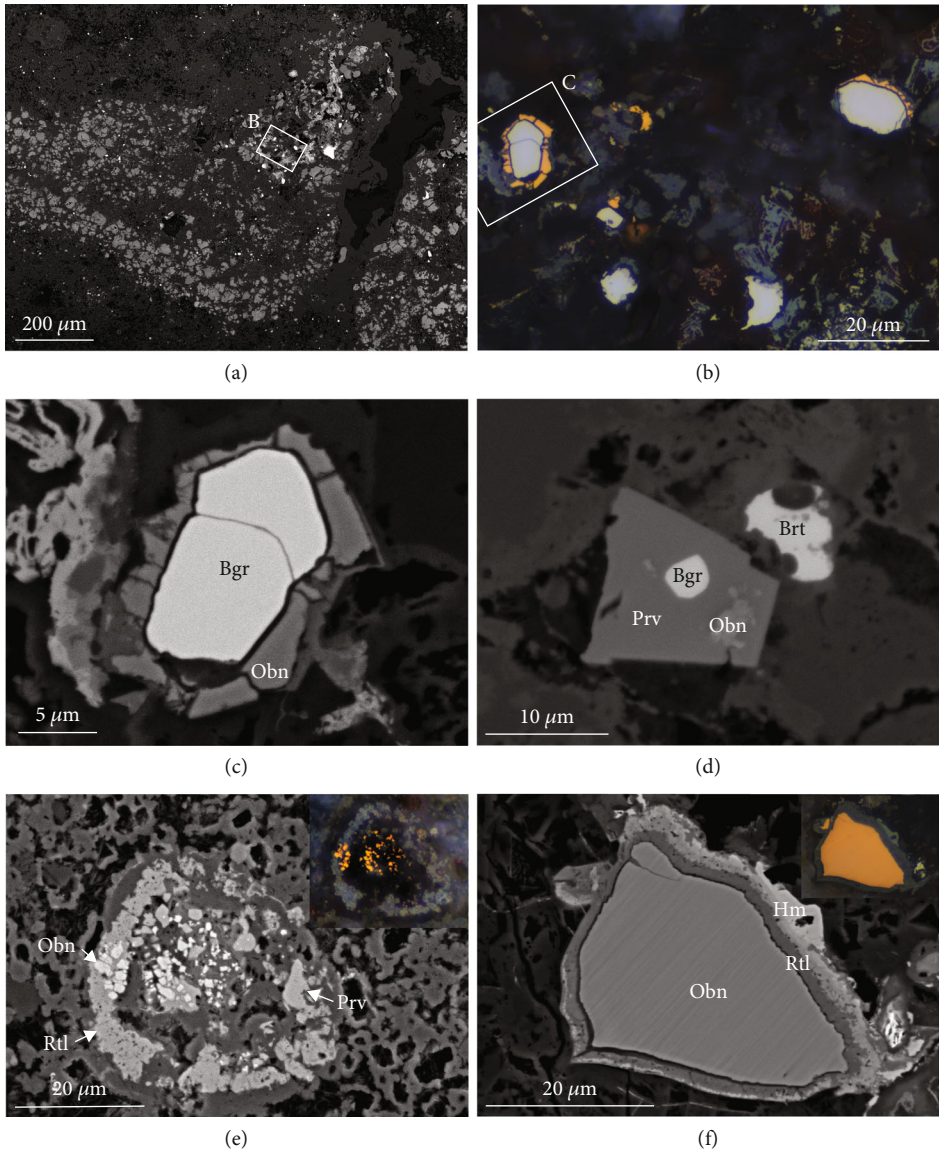

Figure 4: BSE (a, c–f) images and optical microscopy (b, e (inset), f (inset)) of osbornite occurrences. (a) Apophysis of paralava enriched in pseudowollastonite in hydrogrossular-bearing host rock. The magnified area in (B) is shown in the frame. (b) Small osbornite grains are identified by gold color in reflected light. The magnified area in (C) is shown in frame. (c) Osbornite rim on barringerite grain. (d) Osbornite and barringerite inclusions in perovskite from the centre of a small host rock clast. (e) Osbornite relics in rutile and perovskite. (f) Osbornite crystal rimmed by rutile and hematite. Bgr = barringerite; Brt = baryte; Hm = hematite; Obn = osbornite; Prv = perovskite; Rtl = rutile; Scb = schreibersite.

phosphides (Figures 1(b), 1(c), and 3). Osbornite has not been observed within larger host rock clasts or gehlenite paralava. In the narrow tongue of the paralava enriched in pseudowollastonite, many small grains of osbornite were found, which are clearly distinguishable due to their golden color under the optical microscope (Figures 4(a) and 4(b)).

In rare cases, osbornite is partially replaced by rutile, and it is observed as inclusions in perovskite (Figures 4(d)–4(f)). It should be underlined that osbornite from the all known "terrestrial" findings does not carry features of secondary alterations [29–33, 41, 42, 44].

Grains of osbornite have also been observed within central parts of small clasts of host rock, where they form intergrowths with perovskite, murashkoite, and barringerite (Figure 5). Osbornite crystal morphology and mineral associations vary from xenomorphic (Figure 1(c)) to skeletal grains (Figures 3(e) and 5(d)); intergrowths with barringerite, schereibersite, and Cr-bearing pyrrhotite (Figures 3(c), 3(d), and 5(e)); and rims around barringerite (Figure 4(c)). Osbornite is also found in association with graphite (Figure 5(e)) [46] and paqueite; the latter of which only occurs at the narrow contact zone of hydrogrossular fragments (Figures 5(b) and 5(f)). Paqueite is a new mineral discovered within refractive inclusions of the Allende meteorite [63, 64] and has the stoichiometric formula, $Ca_3Ti^{4+}_{1.00}Si_{2.00}(Al_{2.00}Ti^{4+}_{0.75}Si_{0.25})_{\sum 3}O_{14}$, in our samples. In rare cases, osbornite is partially replaced by rutile and may form inclusions in perovskite (Figures 4(d)–4(f)).

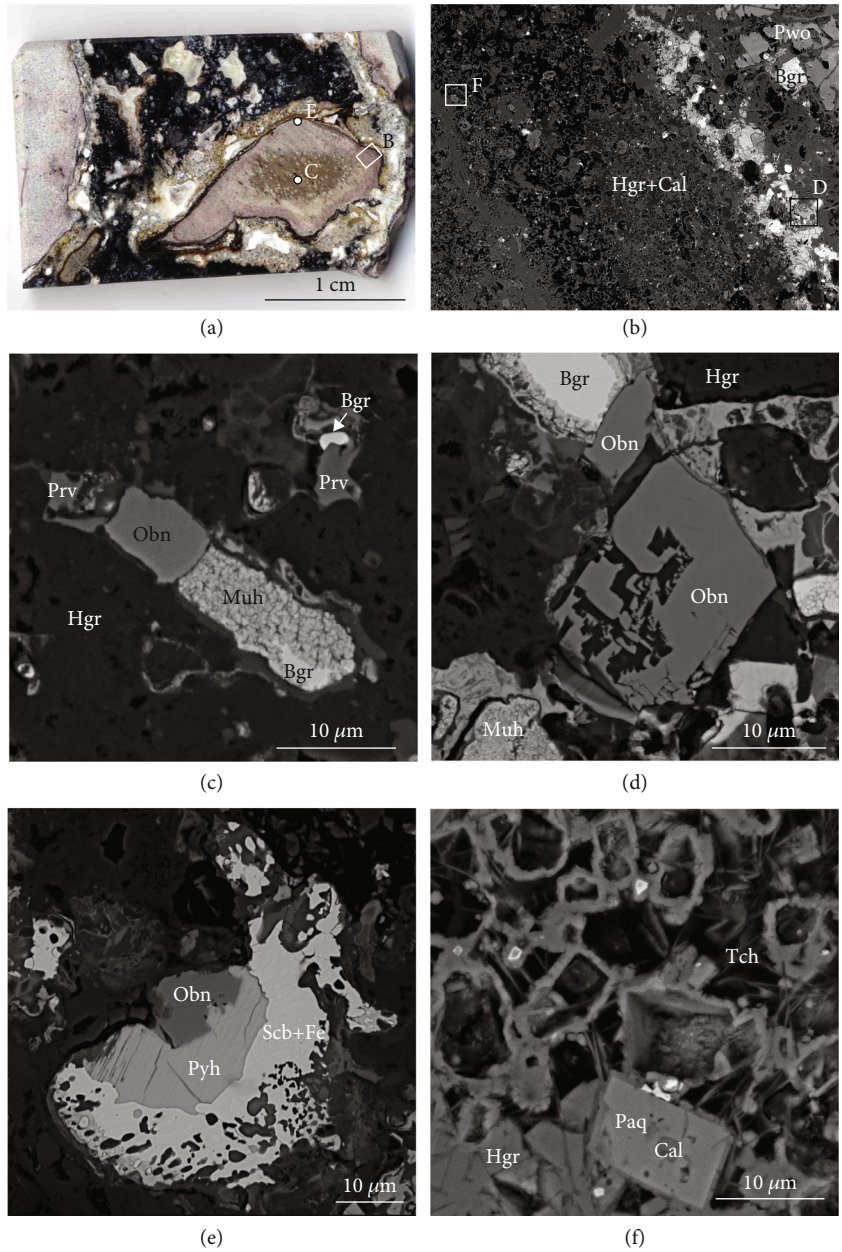

Figure 5: Scanned section (a) and BSE (b–f) images of osbornite and its mineral associations within a host rock clast. (a) Small fragment of hydrogrossular-bearing rock in paralava. The magnified area in (B) is shown in the frame, and areas magnified in (C) and (E) are shown by white spots. (b) Contact of hydrogrossular rock and paralava. Areas magnified in (D) and (F) are shown in the frame. (c) Osbornite intergrows with spongy aggregate of murashkoite in clast centre. (d) Skeletal osbornite. (e) Osbornite intergrowth with pyrrhotite and schreibersite-iron eutectic. (f) Paqueite in porous hydrogrossular rock. Bgr = barringerite; Cal = calcite; Fe = native iron; Hgr = hydrogrossulare; Muh = murashkoite; Obn = osbornite; Paq = paqueite; Prv = perovskite; Pwo = pseudowollastonite; Pyh = pyrrhotite; Scb = schreibersite; Tch = tacharanite.

4. Osbornite Chemistry and Crystal Structure

Although there is some variability between grains, osbornite composition is close to stoichiometric TiN (Table 1). It contains impurities of V (up to 2.56 wt.%), Ca (up to 2.41 wt.%), Cr (up to 1.09 wt.%), and Fe (up to 0.89 wt.%) (Table 1). The main bands in the Raman spectrum of osbornite are as follows (Figure 6): 569 cm^{-1} (TO-transverse optical mode), 319 cm^{-1} (LA-longitudinal acoustic), and 221 cm^{-1} (TA-first-order transverse acoustic) and shoulder about 452 cm^{-1} (2A-second-order acoustic) [65]. The position of band 221 cm^{-1} is related to stoichiometric cubic TiN (*Fm*-3 m, $a = 4.24$ Å); in synthetic phases with composition $TiN_{0.55}$ (*Fm*-3 m, $a = 4.22$ Å), its band shifts to 250 cm^{-1} [66].

Single-crystal X-ray diffraction was performed on the grain shown in Figure 1(c) and confirms the crystal structure of osbornite presented by stoichiometric phase TiN (*Fm*-3 m, $a = 4.24295(19)$; Tables 2–4).

Table 1: Chemical composition of osbornite from the Hatrurim Basin, wt.%.

	$n = 14^*$	s.d.	Range	$n = 13^{**}$	s.d.	Range
Ti	74.39	1.32	70.72-75.75	74.11	1.07	71.42-75.70
Si	0.13	0.06	0.06-0.29	0.15	0.07	0.05-0.28
V	0.74	0.74	0-2.25	0.78	0.76	0-2.56
Cr	0.73	0.24	0.38-1.09	0.72	0.24	0.36-1.09
Fe	0.49	0.17	0.30-0.89	0.49	0.15	0.28-0.76
Al	0.04	0.02	0.03-0.10	0.04	0.00	0.03-0.05
Ca	0.96	0.46	0.61-2.41	0.98	0.37	0.60-1.88
N	22.51	0.64	21.80-24.55	23.81	1.67	21.75-26.78
Total	100.00			101.07		
			Calculated on 2 atoms			
Ti	0.96			0.93		
Ca	0.01			0.01		
V	0.01			0.01		
Cr	0.01			0.01		
Fe	0.01			0.01		
N	1.00			1.02		

$^*N$ calculated as differential element to 100%, $^{**}N$ measured, BN standard.

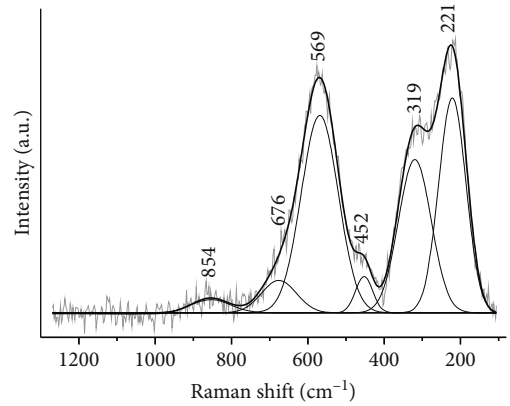

Figure 6: Raman spectrum of the osbornite grain.

5. Origin of Natural Terrestrial Osbornite

The origin of naturally occurring terrestrial osbornite, and its association with highly reduced conditions [41], needs to be diligently assessed due to the significant potential for contamination of geological samples by anthropogenic analogues. In most technological processes, titanium nitride coating is produced at temperature above 1000°C and under reducing conditions in a nitrogen atmosphere using physical or chemical vapor deposition [20]. In contrast, crystallization of extraterrestrial osbornite occurs at high temperatures (>1500°C), super-reduced conditions, i.e., fO_2< iron-wüstite buffer (ΔIW) ≈ −6 [35, 38] and in the presence of fluid (gas, plasma) [67].

Our observations of *in situ* osbornite forming in association with typical meteoritic phosphides in explosive breccias of the Hatrurim Complex (e.g., Figures 1(c), 2(c)–2(e), 4(c), 5(c), and 5(e)) thus imply high-temperature and super-reduced physicochemical conditions of crystallization, which are rarely achieved in the Earth's crust. Such reduced conditions are also unusual for other occurrences of gehlenite paralava in the Hatrurim Basin, which contain Fe^{3+}-bearing minerals [52]. As the majority of osbornite crystals were found in pseudowollastonite-rich zones together with phosphides at the rock contact (Figures 3(c), 3(d), 4(c), and 5(b)–5(e)), we can use osbornite as a tracer mineral for petrogenesis. A likely source of the reducing agent (graphite-like carbon) is the pyrolytic decomposition of bitumen in the sedimentary protolith of the Hatrurim Complex, which also played a significant role in the formation of phosphides and became a source of nitrogen. Osbornite formation here can be tentatively assigned to the following reaction involving carbothermic reduction and nitridation of titanium oxide: $TiO_2 + N + C = TiN + CO_2(g)$ [68, 69]. In addition, the presence of graphite intimately associated with osbornite (Figure 5(e)) is evidence of the highly reduced formations conditions.

Table 2: Data collection and structure-refinement details for osbornite.

Crystal system	Cubic
Unit cell dimensions (Å)	$a = 4.24295(19)$
Space group	*Fm*-3 m (225)
Volume (Å^3)	76.384 (10)
Z	4
Density (calculated) (g/cm^3)	5.384
Crystal size (μm)	18 × 19 × 7
Data collection	
Diffractometer	SuperNova MoKα 0.71073293 (2)
X-ray power	50 kV, 0.8 mA
Detector	Atlas CCD (Agilent Technologies)
Max. θ range for data collection (°)	25.798
Index ranges	$-5 < h < 4$ $-5 < k < 5$ $-5 < l < 5$
No. of measured reflections	168
No. of unique reflections	11
Refinement of the structure	
No. of parameters	3
R_{int}	0.0101
$R1_{(obs)}/R1_{(all)}$	0.0129/0.0129
$wR2_{(obs)}/wR2_{(all)}$	0.0277/0.0277
$GOF_{(obs)}/GOF_{(all)}$	1.361
$\Delta\rho$ min. ($-e$.Å^{-3})	-0.358
$\Delta\rho$ max. (e.Å^{-3})	0.280

Table 3: Atom coordinates, U^{eq} (Å2), anisotropic displacement parameters U^{ij} for osbornite.

Site	Atom	x/a	y/b	z/c	U^{eq}	U^{11}	U^{22}	U^{33}	U^{23}	U^{13}	U^{12}
Ti1	Ti	0	0	0	0.0029 (6)	0.0029 (6)	0.0029 (6)	0.0029 (6)	0	0	0
N1	N	0.5	0.5	0.5	0.0034 (15)	0.0034 (15)	0.0034 (15)	0.0034 (15)	0	0	0

Table 4: Interatomic distances (Å) for osbornite.

Atom	-Atom	Distance
Ti	N	2.1215 (1)
Ti	Ti	3.0002 (1)

A similar process has been proposed for the recent discovery of V-Cr-bearing allabogdanite and V-bearing andreyivanovite associating with barringerite and schreibersite in the pseudowollastonite-enriched zone in the studied wadi Zohar breccia, with phosphide forming via a high-temperature carbothermal reduction process involving gaseous products from decomposition of organic matter at low pressures and high temperatures 1200-1500°C [46]. In this case, geochemical data suggest that the gehlenite paralava and altered rock clasts in breccia were likely derived from the same sedimentary protolith [46]. The latter is speculated to contain layers or lenses enriched in phosphorite-like materials, namely, the P-Si-Fe and P-Si-C series with a carbonate-argillaceous cement, analogous to the lithological units at the unconformable boundaries between the Campanian Mishash and the Maastrichtian bituminous Ghareb formations (major protolith unit of the Hatrurim Complex) [46, 70]. The sedimentary protolith was initially calcinated and transformed to a clinker-like rock; therefore, we propose that in our case, the main reducing agents during phosphide formation were not bitumen materials but products of its pyrolytic decomposition, i.e., graphite-like substances with admixtures of sulfur and nitrogen. Moreover, the formation temperature of gehlenite paralava was potentially as high as 1500°C and was likely maintained by gaseous fluxes which were instrumental in melting of the contact sedimentary rocks and accumulation of liquid droplets of native Fe, which subsequently formed complex aggregates with phosphides (Figure 2(a)) [46]. The process of iron and phosphorus reduction and phosphide formation can be described by the following reactions:

$$\mathrm{Fe_2O_3 + 3C \longrightarrow 2Fe(lq) + 3CO(g)}$$

$$\mathrm{8Ca_5(PO_4)_3F + 22SiO_2 + 20Al_2O_3 + 60C = 12P_2(g) + 60CO + 20Ca_2Al_2O_7 + 2SiF_4(g)}$$

$$\mathrm{nFe(lq) + \frac{1}{2}P_2(g) = Fe_nP,} \quad (1)$$

where $n = 1, 2, 3$ [46].

In conclusion, we document the first unquestionable evidence for terrestrial origins of natural osbornite from phosphide-bearing breccia in the Hatrurim Complex, Israel. The conditions of formation and mineral association of osbornite, in contrast to other osbornite findings, are similar to those in meteorites.

Data Availability

All data generated during this study are included in this published article and its supplementary materials. Original data are available on request from the corresponding author.

Conflicts of Interest

The authors declare that they have no conflicts of interest.

Acknowledgments

Investigations were supported by the National Science Center of Poland Grant (grant number 2021/41/B/ST10/00130).

Supplementary Materials

Table S1: chemical composition of Fe-P (±C) mineral aggregate: baringerrite (1, core), schreibersite (2, intermediate zone), eutectic zone (rim): schreibersite (3), cohenite (4), and iron (5), wt.%. Figure S1: rankinite-gehlenite paralava with flamite relics. (A) BSE and (B) cathodoluminescence (CL). Rounded relics of flamite are poorly defined in rankinite in the BSE image. Like gehlenite, flamite does not luminesce, so its rounded relics are clearly visible in luminescent rankinite in CL image. Fmt = flamite; Gh = gehlenite; Pyh = pyrrhotite; Rnk = rankinite. *(Supplementary Materials)*

References

[1] M. R. Lee, S. S. Russel, J. W. Arden, and C. T. Pillinger, "Nierite (Si3N4), a new mineral from ordinary and enstatite chondrites," *Meteoritics & Planetary Science*, vol. 30, no. 4, pp. 387–398, 1995.

[2] K. Keil and C. A. Andersen, "Occurrences of sinoite, Si_2N_2O, in meteorites," *Nature*, vol. 207, no. 4998, p. 745, 1965.

[3] V. F. Buchwald and H. P. Nielsen, "Roaldite, a new nitride in iron meteorites," *Lunar and Planetary Science*, vol. 12, pp. 112–114, 1981.

[4] V. F. Buchwald and E. R. D. Scott, "First nitride (CrN) in iron meteorites," *Nature Physical Science*, vol. 233, no. 41, pp. 113-114, 1971.

[5] V. V. Sharygin, G. S. Ripp, G. A. Yakovlev et al., "Uakitite, VN, a new mononitride mineral from Uakit iron meteorite (IIAB)," *Minerals*, vol. 10, no. 2, p. 150, 2020.

[6] F. A. Bannister, "Osbornite, meteoritic titanium nitride," *Mineralogical Magazine*, vol. 26, no. 173, pp. 36–44, 1941.

[7] S. Bette, T. Theye, H.-J. Bernhardt, W. P. Clark, and R. Niewa, "Confirmation of siderazot, $Fe_3N_{1.33}$, the only terrestrial nitride mineral," *Minerals*, vol. 11, no. 3, p. 290, 2021.

[8] L. Bindi, F. Cámara, S. E. M. Gain et al., "Kishonite, VH_2, and oreillyite, Cr_2N, two new minerals from the corundum xenocrysts of Mt Carmel, northern Israel," *Minerals*, vol. 10, no. 12, p. 1118, 2020.

[9] L. F. Dobrzhinetskaya, R. Wirth, J. Yang et al., "Qingsongite, natural cubic boron nitride: the first boron mineral from the Earth's mantle," *American Mineralogist*, vol. 99, no. 4, pp. 764–772, 2014.

[10] G. Tunell, J. J. Fahey, F. W. Daugherty, and G. V. Gibbs, *Gianellaite, a New Mercury Mineral*, Neues Jahrbuch für Mineralogie, Monatshefte, 1977.

[11] A. Sachs, *Der kleinit, ein hexagonales quecksilberoxychlorid von Terlingua in Texas*, Sitzungsberichte der Königlich Preussischen Akademie der Wissenschaften, 1905.

[12] F. A. Canfield, W. F. Hillebrand, and W. T. Schaller, "Mosesite, a new mercury mineral from Terlingua, Texas," *American Journal of Science*, vol. 30, pp. 202–208, 1910.

[13] A. C. Roberts, H. G. Ansell, and P. J. Dunn, "Comancheite, a new mercury oxychloride-bromide from Terlingua, Texas," *Canadian Mineralogist*, vol. 19, pp. 393–396, 1981.

[14] M. K. Weisberg, M. Prinz, and C. E. Nehru, "Petrology of ALH85085: a chondrite with unique characteristics," *Earth and Planetary Science Letters*, vol. 91, no. 1-2, pp. 19–32, 1988.

[15] V. I. Grokhovsky, "Osbornite in Cb/Ch-like carbonaceous chondrite Isheyevo," *Meteoritics & Planetary Science*, vol. 41, no. 8, p. A68, 2006.

[16] J. Leitner, C. Vollmer, and P. Hoppe, "A study of osbornite from enstatite chondrites at the submicrometer scale," in *49th Lunar and Planetary Science Conference 2018 (LPI Contrib. No. 2083)*, The Woodlands, TX, USA, 2018.

[17] M. E. Zolensky, T. J. Zega, H. Yano et al., "Mineralogy and petrology of comet 81P/wild 2 nucleus samples," *Science*, vol. 314, no. 5806, pp. 1735–1739, 2006.

[18] L. E. Toth, *Transition Metal Carbides and Nitrides*, Academic Press, New York, 1971.

[19] W. Lengauer, "Transition metal carbides, nitrides, and carbonitrides," in *Handbook of Ceramic Hard Materials*, R. Riedel, Ed., pp. 202–252, WILEY-VCH Verlag Gmb H, 2000.

[20] M. Azadi, A. Sabour Rouhaghdam, and S. Ahangarani, "A review on titanium nitride and titanium carbide single and multilayer coatings deposited by plasma assisted chemical vapor deposition," *International Journal of Engineering, Transactions B: Applications*, vol. 29, pp. 677–687, 2016.

[21] Y. Erokhin, V. V. Khiller, and L. A. Zakharova, ""Cosmic" mineralogy in metallurgical slags of the Urals," *Mineralogy of Technogenesis*, vol. 2017, pp. 72–81, 2017.

[22] A. M. Koverzin, A. B. Vaschenko, A. S. Bluzniukov, R. Satradinov, A. P. Makavetskac, and Y. A. Fischenko, "Investigation of the skull and lining in the blast furnace hearth," *Bulletin "Black Metallurgy"*, vol. 8, pp. 17–29, 2018.

[23] E. Lucas, P. Drillet, and G. Boi, "TiN formation in steels depending of titanium and nitrogen," *Metallurgical Research & Technology*, vol. 116, no. 5, p. 516, 2019.

[24] S. K. Michelic and C. Bernhard, "Experimental Study on the Behavior of TiN and Ti_2O_3 Inclusions in Contact with CaO-Al_2O_3-SiO_2-MgO Slags," *Scanning*, vol. 2017, Article ID 2326750, 2017.

[25] C. Milton and D. B. Vitaliano, "The non-existence of moissanite, SiC," *International Geological Congress*, vol. 27, no. 5, pp. 107-108, 1984.

[26] K. D. Litasov, H. Kagi, S. A. Voropaev et al., "Comparison of enigmatic diamonds from the Tolbachik arc volcano (Kamchatka) and Tibetan ophiolites: assessing the role of contamination by synthetic materials," *Gondwana Research*, vol. 75, pp. 16–27, 2019.

[27] K. D. Litasov, H. Kagi, and T. B. Bekker, "Enigmatic super-reduced phases in corundum from natural rocks: possible contamination from artificial abrasive materials or metallurgical slags," *Lithos*, vol. 340-341, pp. 181–190, 2019.

[28] V. I. Tatarintsev, S. M. Sandomirskaya, and S. N. Tsumbal, "First discovery of titanium nitride (osbornite) in terrestrial rocks," *Doklady USSR Academy of Sciences*, vol. 296, pp. 1458–1461, 1987.

[29] L. F. Dobrzhinetskaya, W. Wirth, J. Yang, I. D. Hutcheon, P. K. Weber, and H. W. Green, "High-pressure highly reduced nitrides and oxides from chromitite of a Tibetan ophiolite," *Proceedings of the National Academy of Sciences*, vol. 106, no. 46, pp. 19233–19238, 2009.

[30] X. Xu, J. Yang, G. Guo, and F. Xiong, "Mineral inclusions in corundum from chromitites in the Kangjinla chromite deposit, Tibet," *Acta Petrologica Sinica*, vol. 29, pp. 1867–1877, 2013.

[31] Q. Xiong, W. L. Griffin, J.-H. Huang et al., "Super-reduced mineral assemblages in "ophiolitic" chromitites and peridotites: the view from Mount Carmel," *European Journal of Mineralogy*, vol. 29, no. 4, pp. 557–570, 2017.

[32] F. Xiong, X. Xu, E. Mugnaioli et al., "Two new minerals, badengzhuite, TiP, and zhiqinite, TiSi 2, from the Cr-11 chromitite orebody, Luobusa ophiolite, Tibet, China: is this evidence for super-reduced mantle-derived fluids?," *European Journal of Mineralogy*, vol. 32, no. 6, pp. 557–574, 2020.

[33] F. Xiong, X. Xu, E. Mugnaioli et al., "Jingsuiite, TiB_2, a new mineral from the Cr-11 podiform chromitite orebody, Luobusa ophiolite, Tibet, China: implications for recycling of boron," *American Mineralogist*, vol. 107, no. 1, pp. 43–53, 2022.

[34] S. M. Drake, A. D. Beard, A. P. Jones et al., "Discovery of a meteoritic ejecta layer containing unmelted impactor fragments at the base of Paleocene lavas, Isle of Skye, Scotland," *Geology*, vol. 46, no. 2, pp. 171–174, 2018.

[35] W. L. Griffin, S. E. M. Gain, D. T. Adams et al., "First terrestrial occurrence of tistarite (Ti_2O_3): ultra-low oxygen fugacity in the upper mantle beneath Mount Carmel, Israel," *Geology*, vol. 44, no. 10, pp. 815–818, 2016.

[36] W. L. Griffin, J.-X. Huang, E. Thomassot, S. E. M. Gain, V. Toledo, and S. Y. O'Reilly, "Super-reducing conditions in ancient and modern volcanic systems: sources and behaviour of carbon-rich fluids in the lithospheric mantle," *Mineralogy and Petrology*, vol. 112, no. S1, pp. 101–114, 2018.

[37] W. L. Griffin, S. E. M. Gain, L. Bindi et al., "Carmeltazite, ZrAl2Ti4O11, a new mineral trapped in corundum from volcanic rocks of Mt Carmel, northern Israel," *Minerals*, vol. 8, no. 12, p. 601, 2018.

[38] W. L. Griffin, S. E. M. Gain, J.-H. Huang et al., "A terrestrial magmatic hibonite-grossite-vanadium assemblage: desilication and extreme reduction in a volcanic plumbing system, Mount Carmel, Israel," *American Mineralogist*, vol. 104, no. 2, pp. 207–219, 2019.

[39] W. L. Griffin, S. E. M. Gain, M. Saunders et al., "Parageneses of TiB_2 in corundum xenoliths from Mt. Carmel, Israel:

siderophile behavior of boron under reducing conditions," *American Mineralogist*, vol. 105, no. 11, pp. 1609–1621, 2020.

[40] W. L. Griffin, S. E. M. Gain, F. Cámara et al., "Extreme reduction: mantle-derived oxide xenoliths from a hydrogen-rich environment," *Lithos*, vol. 358-359, article 105404, 2020.

[41] W. L. Griffin, S. E. M. Gain, M. Saunders et al., "Nitrogen under super-reducing conditions: Ti oxynitride melts in xenolithic corundum aggregates from Mt Carmel (N. Israel)," *Minerals*, vol. 11, no. 7, p. 780, 2021.

[42] V. I. Silaev, G. A. Karpov, N. P. Anikin, L. P. Vergasova, V. N. Fillipov, and K. V. Tarasov, "Mineral phase paragenesis in explosive ejecta discharged by recent eruptions in Kamchatka and on the Kuril Islands. Part 2. Accessory minerals of the Tolbachik type diamonds," *Volcanology Seismology*, vol. 13, no. 6, pp. 376–388, 2019.

[43] I. G. Yatsenko, S. G. Skublov, E. V. Levashova, O. L. Galankina, and S. N. Bekesha, "Composition of spherules and lower mantle minerals, isotopic and geochemical characteristics of zircon from volcaniclastic facies of the Mriya lamproite pipe," *Journal of Mining Institute*, vol. 242, pp. 150–159, 2020.

[44] I. G. Yatsenko, O. L. Galankina, Y. B. Marin, and S. G. Skublovb, "Corundum with inclusions of extremely reduced minerals from explosive rocks of the Ukrainian shield," *Doklady Earth Sciences*, vol. 500, no. 2, pp. 833–837, 2021.

[45] C. Ballhaus, H. M. Helmy, R. O. C. Fonseca, R. Wirth, A. Schreiber, and N. Jöns, "Ultra-reduced phases in ophiolites cannot come from Earth's mantle," *American Mineralogist*, vol. 106, no. 7, pp. 1053–1063, 2021.

[46] E. V. Galuskin, J. Kusz, I. O. Galuskina, M. Książek, Y. Vapnik, and G. Zieliński, "Discovery of terrestrial andreyivanovite, FeCrP, and the effect of Cr and V substitution in barringerite-allabogdanite low-pressure transition," *American Mineralogist*, 2023, in press.

[47] S. Gross, *The Mineralogy of the Hatrurim Formation, Israel*, Geological Survey of Israel, Jerusalem, Israel, 1977.

[48] A. Burg, Y. Kolodny, and V. Lyakhovsky, "Hatrurim-2000: the "mottled zone" revisited, forty years later," *Israel Journal of Earth Sciences*, vol. 48, pp. 209–223, 1999.

[49] Y. Vapnik, V. V. Sharygin, E. V. Sokol, and R. Shagam, "Paralavas in a combustion metamorphic complex: Hatrurim Basin, Israel," *Reviews in Engineering Geology*, vol. 18, pp. 1–21, 2007.

[50] I. Novikov, E. Vapnik, and I. Safonova, "Mud volcano origin of the mottled zone, South Levant," *Geoscience Frontiers*, vol. 4, no. 5, pp. 597–619, 2013.

[51] S. N. Britvin, M. N. Murashko, Y. Vapnik et al., "Cyclophosphates, a new class of native phosphorus compounds, and some insights into prebiotic phosphorylation on early Earth," *Geology*, vol. 49, no. 4, pp. 382–386, 2021.

[52] I. O. Galuskina, E. V. Galuskin, A. S. Pakhomova et al., "Khesinite, Ca4Mg2Fe3+ 10O4[(Fe3+ 10Si2)O36], a new rhönite-group (sapphirine supergroup) mineral from the Negev Desert, Israel– natural analogue of the SFCA phase," *European Journal of Mineralogy*, vol. 29, no. 1, pp. 101–116, 2017.

[53] E. Sokol, I. Novikov, S. Zateeva, Y. Vapnik, R. Shagam, and O. Kozmenko, "Combustion metamorphism in the Nabi Musa dome: new implications for a mud volcanic origin of the mottled zone, Dead Sea area," *Basin Research*, vol. 22, no. 4, pp. 414–438, 2010.

[54] S. N. Britvin, M. N. Murashko, Y. Vapnik, Y. S. Polekhovsky, and S. V. Krivovichev, "Earth's phosphides in Levant and insights into the source of Archean prebiotic phosphorus," *Scientific Reports*, vol. 5, no. 1, p. 8355, 2015.

[55] E. V. Galuskin, I. O. Galuskina, F. Gfeller et al., "Silicocarnotite, Ca5 [(SiO4)(PO4)](PO4), a new „old" mineral from the Negev Desert, Israel, and the ternesite–silicocarnotite solid solution: indicators of high-temperature alteration of pyrometamorphic rocks of the Hatrurim Complex, Southern Levant," *European Journal of Mineralogy*, vol. 28, no. 1, pp. 105–123, 2016.

[56] E. Galuskin, I. Galuskina, Y. Vapnik, and M. Murashko, "Molecular hydrogen in natural mayenite," *Minerals*, vol. 10, no. 6, p. 560, 2020.

[57] S. N. Britvin, Y. Vapnik, Y. S. Polekhovsky et al., "Murashkoite, FeP, a new terrestrial phosphide from pyrometamorphic rocks of the Hatrurim Formation, South Levant," *Mineralogy and Petrology*, vol. 113, no. 2, pp. 237–248, 2019.

[58] S. N. Britvin, M. N. Murashko, Y. E. Vapnik et al., "Transjordanite, Ni2P, a new terrestrial and meteoritic phosphide, and natural solid solutions barringerite-transjordanite (hexagonal Fe2P–Ni2P)," *American Mineralogist*, vol. 105, no. 3, pp. 428–436, 2020.

[59] S. N. Britvin, M. N. Murashko, Y. Vapnik et al., "Halamishite, Ni5P4, a new terrestrial phosphide in the Ni–P system," *Physics and Chemistry of Minerals*, vol. 47, no. 1, p. 3, 2020.

[60] G. M. Sheldrick, "Crystal structure refinement withSHELXL," *Acta Crystallographica Section C: Structural Chemistry*, vol. 71, no. 1, pp. 3–8, 2015.

[61] A. Burg, A. Starinsky, Y. Bartov, and Y. Kolodny, "Geology of the Hatrurim Formation ("mottled zone") in the Hatrurim Basin, Israel," *Journal of Earth Science*, vol. 40, pp. 107–124, 1991.

[62] Y. Vapnik, V. Palchik, I. Galuskina, K. Banasik, and T. Krzykawski, "Mineralogy, chemistry and rock mechanic parameters of katoite-bearing rock from the Hatrurim Basin, Israel," *Journal of African Earth Sciences*, vol. 147, pp. 322–330, 2018.

[63] J. M. Paque, J. R. Beckett, D. J. Barber, and E. M. Stolper, "A new titanium-bearing calcium aluminosilicate phase: I. meteoritic occurrences and formation in synthetic systems," *Meteoritics*, vol. 29, no. 5, pp. 673–682, 1994.

[64] C. Ma, J. R. Beckett, F. L. H. Tissot, and G. R. Rossman, "New minerals in type A inclusions from Allende and clues to processes in the early solar system: paqueite, $Ca_3TiSi_2(Al,Ti,-Si)_3O_{14}$, and burnettite, $CaVAlSiO_6$," *Meteoritics & Planetary Science*, vol. 57, no. 6, pp. 1300–1324, 2022.

[65] Y. H. Cheng, B. K. Tay, S. P. Lau, H. Kupfer, and F. Richter, "Substrate bias dependence of Raman spectra for TiN films deposited by filtered cathodic vacuum arc," *Journal of Applied Physics*, vol. 92, no. 4, pp. 1845–1849, 2002.

[66] W. Spengler, R. Kaiser, A. N. Christensen, and G. Müller-Vogt, "Raman scattering, superconductivity, and phonon density of states of stoichiometric and nonstoichiometric TiN," *Physical Review B*, vol. 17, p. 1095, 1976.

[67] A. Meibom, A. N. Krot, F. Robert et al., "Nitrogen and carbon isotopic composition of the sun inferred from a high-temperature solar nebular condensate," *Astrophysical Journal*, vol. 656, no. 1, pp. L33–L36, 2007.

[68] G. V. White, K. J. D. Mackenzie, and J. H. Johnston, "Carbothermal synthesis of titanium nitride," *Journal of Materials Science*, vol. 27, no. 16, pp. 4287–4293, 1992.

[69] W. Yu, X. Wen, W. Liu, and J. Chen, "Carbothermic reduction and nitridation mechanism of vanadium-bearing titanomagnetite concentrate," *Minerals*, vol. 11, no. 7, p. 730, 2021.

[70] Y. Shahar, N. Yaacov, and S. Yair, "Two close associations : Si-P-Fe and Si-P-C in the upper Campanian and lower Maastrichtian sediments of the Negev, Israel. Deux paragenèses associées : Si-P-Fe et Si-P-C dans les sédiments du Campanien supérieur et du Maastrichtien inférieur du Néguev, Israël," *Sciences Géologiques Bulletins*, vol. 42, no. 3, pp. 155–171, 1989.